GPS radio sources

Labiano, A.; Barthel, P. D.; O'Dea, C. P.; Vries, W. H. de; Pérez, I; Baum, S. A.

Published in:
Astronomy & Astrophysics

DOI:
10.1051/0004-6361:20066183

Publication date:
2007

A&A 463, 97–104 (2007)
DOI: 10.1051/0004-6361:20066183

Astronomy & Astrophysics

GPS radio sources: new optical observations and an updated master list⋆

A. Labiano[1,2], P. D. Barthel[1], C. P. O'Dea[3], W. H. de Vries[4,5], I. Pérez[1], and S. A. Baum[6]

[1] Kapteyn Astronomical Institute, Groningen, 9700 AV, The Netherlands
e-mail: labiano@damir.iem.csic.es
[2] Departamento de Astrofísica Molecular e Infrarroja, Instituto de Estructura de la Materia (CSIC), Madrid, Spain
[3] Department of Physics, Rochester Institute of Technology, Rochester, NY 14623, USA
[4] University of California, Davis, CA 95616, USA
[5] Lawrence Livermore National Laboratory / IGPP, Livermore, CA 94550, USA
[6] Center for Imaging Science, Rochester Institute of Technology, Rochester, NY 14623, USA

Received 4 August 2006 / Accepted 9 November 2006

ABSTRACT

Aims. We identify optical counterparts, address uncertain identifications and measure previously unknown redshifts of the host galaxies of candidate GPS radio sources, and study their stellar populations.
Methods. Long slit spectroscopy and deep optical imaging in the B, V and R bands, obtained with the Very Large Telescope.
Results. We obtain new redshifts for B0316+161, B0407–658, B0904+039, B1433–040, and identify the optical counterparts of B0008–421 and B0742+103. We confirm the previous identification for B0316+161, B0407–658, B0554–026, and B0904+039, and find that the previous identification for B0914+114 is incorrect. Using updated published radio spectral information, we classify as non GPS the following sources: B0407–658, B0437–454, B1648+015. The optical colors of typical GPS sources are consistent with single instantaneous burst stellar population models but do not yield useful information on age or metallicity. A new master list of GPS sources is presented.

Key words. galaxies: active – galaxies: distances and redshifts – galaxies: quasars: emission lines – galaxies: general

1. Introduction

GigaHertz Peaked Spectrum (GPS) radio sources are fairly common – O'Dea (1998) lists a 10% fraction in high frequency selected catalogs. In the current paradigm, the extended radio galaxies and quasars are unified with the compact, core-dominated quasars and BL Lac-objects through the combined effects of radio jet orientation and anisotropic obscuration (e.g., Urry & Padovani 1995). These objects are considered to be mature, well developed radio sources. It is likely that GPS objects are young radio sources that will evolve into the 10–100 kpc scale objects. Studies of radio galaxy evolution suggest that the GPS sources can evolve into the larger scale radio galaxies, dimming in radio luminosity as they expand (e.g., Fanti et al. 1995; Begelman 1996; Readhead et al. 1996; De Young 1997; Kaiser et al. 1997; Kaiser & Alexander 1997; O'Dea & Baum 1997; Snellen et al. 2000). Multi-color optical as well as near-IR imaging (e.g., O'Dea et al. 1996; Snellen et al. 1996; de Vries et al. 2000a) have shown that host galaxy colors of nearby GPS objects are indeed consistent with non- or passively evolving ellipticals, with absolute magnitudes comparable to the brightest cluster members, similar to the hosts of intermediate sized and large radio source classes. Determination of the rest-frame broad-band colors (which requires redshifts) in connection with stellar population synthesis modeling has proven essential for these investigations (e.g., de Vries et al. 2000b).

O'Dea et al. (1991) presented a list of candidate GPS radio sources. About half of those sources had unknown redshifts and several lacked an optical counterpart. The sample has been updated with new identifications and redshifts since then (e.g., de Vries et al. 1997). However, the optically faint part of the sample requires the use of 8 m class telescopes. Our goal in this paper is to increase the number of optical identifications, measure new redshifts and remove non GPS sources from the current samples, using updated radio data from the literature. Using the ESO VLT, we have therefore observed 8 unidentified and 5 tentatively identified objects from the master list of O'Dea et al. (1991).

We here present these observations of sources with unknown or uncertain redshifts or optical counterparts, and increase the number of confirmed GPS sources (up to 74, out of 95 candidates) of the complete O'Dea et al. (1991) list. We give new host identifications (down to $R \sim 25$) and obtain several new redshifts. Using these, as well as literature research and our earlier data, we update the O'Dea et al. (1991) master list. This updated master list is presented in a concluding table. We use $H_0 = 71, \Omega_M = 0.27, \Omega_\Lambda = 0.73$ (Spergel et al. 2003) throughout the paper.

2. Observations and data reduction

The sample was observed during two nights (January 30 to 31, 2000, and December 16 to 17, 2001) using VLT's FORS1/UT1 and FORS2/UT4 (Appenzeller et al. 1998). We obtained long slit spectroscopy using grism 150I with order separators OG590 and GG375, obtaining a 230 Å/mm dispersion (5.52 Å/pixel) and covering wavelengths 6000–11 000 Å (OG590) and 3850–7500 Å (GG375). For the imaging we

⋆ Table 4 is only available in electronic form at http://www.aanda.org

Table 1. Source list and exposure times (in seconds).

Name	Spectroscopy	*B*	*V*	*R*
B0008–421	1800	–	–	600
B0316+161	3000	300	600	–
B0407–658	1500	600	300	300
B0437–454	1800	–	–	–
B0554–026	–	300	300	300
B0742+103	3000	–	–	600
B0904+039	3000	600	300	–
B0914+114	1200[a]	600	480	–
B1045+019	1800	–	–	–
PMN J1300–1059[b]	900	–	–	–
B1433–040	1200	–	–	–
B1601–222	1200	–	–	–
B1648+015	1350	–	–	–

[a] Unrelated galaxy. See notes on individual source for details. [b] PMN J1300–1059 was chosen from the NVSS and WISH surveys (Condon et al. 1998; De Breuck et al. 2002).

used a *R*-Johnson-Cousins filter for the January 2000 run. For the December run, we used the *B*, *V*- Johnson-Cousins and *R*-Special filters[1]. We covered a 6.8 arcmin field with seeing ranging from 0.5″ to 0.7″ for the January run and 0.5″ to 1.1″ for the December run. The pixel scale of FORS is 0.25″/pixel. Table 1 lists the exposure times.

Standard data reduction was performed using IRAF routines. All the spectra were corrected for bias, flat-field and sky subtracted. Wavelength calibration was done using internal arc lamps. The flux calibration and removal of atmospheric lines were performed using the spectrophotometric standards GD50 and GD108.

The calibration of the imaging data was different for the January and December runs. Both runs were corrected for bias and flat-field. The January observations were done during a photometric night. We took flat field images and observed the Landolt (1992) standard fields PG1323–086 and SA 95. No useful standard fields or flat fields were observed for the – non photometric – December run. To correct from flat-field these images, we averaged all the observations in each filter separately to create *artificial* flat-field images, which we used for the correction. As standard stars, we chose unsaturated field stars with data in the Second Guide Star Catalogue (GSC2.2, McLean et al. 1998), about 40 stars in total. The GSC stars have available magnitudes in the photographic *F* and *J* bands. The transformation to the Johnson-Cousins filters was performed following Kent (1985). The January images were taken only in *R*-band. For the December run, most of the standards lacked color information to perform (first order) color coefficient corrections to our apparent magnitudes. We could only fit the zero point magnitudes in each band. The errors on the zero point are: 0.042 for the January observations (*R*-band) and 0.38, 0.17, 0.10 for the December observations (*R*, *B*, *V*-bands respectively).

3. Results

3.1. Identifications

The astrometry was performed using the GSC2.2 catalog as reference. It was possible to make accurate (usually with 1σ error <0.5 arcsec) positional determinations for the candidate optical counterparts. The radio positions are from the VLA calibrator manual (B0008-421, B0316+161, B0742+103) and NED (B0407–658, B0554–026, B0904+039, B0914+114). As in de Vries et al. (1995, 2000b), we use the *likelihood ratio* defined by de Ruiter et al. (1977):

$$R_1 = \sqrt{\frac{\Delta\alpha^2}{\sigma_\alpha^2} + \frac{\Delta\delta^2}{\sigma_\delta^2}} \quad (1)$$

where $\Delta\alpha$ and $\Delta\delta$ are the measured offsets in RA and Dec between the optical and radio positions, σ_α^2 and σ_δ^2 are the sums of the squared 1σ errors in the optical and radio positions. The probability that a true optical counterpart has an R_1 value larger than some R_0 is given by $P(R_1 > R_0) = \mathrm{e}^{-0.5R_0^2}$. An R_1 value less than three indicates a probability of less than 1% of a false identification (assuming that the optical counterpart is the object closest to the radio position). Most of our identifications have R_1 values smaller than 3 and are likely to be correct. The optical position used in the calculation of R_1, and listed in Table 2, corresponds to the center of the source, fitted with IRAF task Ellipse. The identification results are listed in Table 2 and finding charts for the sources are presented in Fig. 4.

3.2. Magnitudes

The magnitudes were extracted performing aperture photometry. We used apertures large enough to include all light from the object (typically a diameter of ∼10 pixels) but minimizing the contribution from sky. The magnitudes are corrected for Galactic extinction, following Schlegel et al. (1998).

B0008–421 and B0742+103 were observed in the *R*-Johnson-Cousins filter in the January 2000 – photometric – night. The photon noise increases the error in magnitude to 0.3 and 0.1 for B0008–421 (with lower signal to noise) and B0742+103 respectively (Table 2).

The rest of the images were taken in the – non photometric – December 2001 run. As judged from internal consistency of field stars with known magnitudes, our photometric accuracy varies between 0.1 and 0.4 mag. The main source of error for this run comes from the uncertainties in the magnitudes of the stars used in the calibration: 0.17, 0.10 and 0.38 for *B*, *V* and *R* bands respectively. A conservative (5σ) detection limit is magnitude ∼25.5 for *R*, *V*-bands and ∼26 for *B*-band, for all sources.

Comparison with the Hubble diagram (O'Dea et al. 1996; Snellen et al. 2002; and Fig. 1) show that the *R*-magnitudes we measure are consistent with previous observations of GPS hosts. The *V*-magnitudes of the new optical counterparts are consistent with those found by di Serego-Alighieri et al. (1994) for hosts of radio sources, although our sources tend to be slightly fainter. We have not found published *B* magnitudes for comparison.

3.3. Spectra and redshifts

We took spectra of 16 sources to measure their redshifts. Table 3 and Fig. 3 show those spectra where emission features were found. We measure redshifts for B0316+161, B0407–658, B0904+039, B1433–040 (with a conservative error of ±0.001) and (the incorrect ID for) B0914+114. Some sources show possible emission lines but their redshifts are uncertain (see notes on each individual object below): B0008–421, PMN J1300–1059, and B1045+019. The spectra were too noisy to find emission features for B0437–454, B0742+103, B1601–222 and B1648+015.

[1] The *R*-Special filter on FORS2 is a Johnson-Cousins filter with a slightly shortened red end to avoid sky emission lines.

Table 2. Positions of the optical counterparts.

	Radio (J2000)		Optical (J2000)			
Source	RA	Dec	RA	Dec	R_1	Magnitude
B0008–421	00:10:52.52	–41:53:10.8	00:10:52.53	–41:53:10.6	2.1	R 24.3 ± 0.3 ± 0.04
B0316+161	03:18:57.80	+16:28:32.7	03:18:57.82	+16:28:32.9	2.0	B 23.0 ± 0.1 ± 0.2
B0316+161	"	"	03:18:57.82	+16:28:32.6	2.0	V 23.4 ± 0.1 ± 0.1
B0407–658	04:08:20.38	–65:45:09.1	04:08:20.37	–65:45:09.0	1.3	B 22.5 ± 0.04 ± 0.2
B0407–658	"	"	04:08:20.41	–65:45:08.6	3.4	V 21.4 ± 0.03 ± 0.1
B0407–658	"	"	04:08:20.41	–65:45:09.4	3.4	R 20.2 ± 0.06 ± 0.4
B0554–026	05:56:52.62	–02:41:05.5	05:56:52.61	–02:41:05.3	2.6	B 18.3 ± 0.01 ± 0.2
B0554–026	"	"	05:56:52.59	–02:41:05.5	3.3	V 17.5 ± 0.02 ± 0.1
B0554–026	"	"	05:56:52.62	–02:41:05.5	3.2	R 16.4 ± 0.01 ± 0.4
B0742+103	07:45:33.06	+10:11:12.7	07:45:33.06	+10:11:12.5	1.9	B 24.0 ± 0.1 ± 0.2
B0742+103	"	"	07:45:33.06	+10:11:12.3	1.9	V 23.8 ± 0.2 ± 0.1
B0742+103	"	"	07:45:32.97	+10:11:12.8	3.9	R 23.1 ± 0.1 ± 0.04
B0904+039	09:06:41.05	+03:42:41.5	09:06:41.03	+03:42:42.0	3.3	V 24.9 ± 0.3 ± 0.1
B0914+114	09:17:16.39	+11:13:36.5	09:17:16.53	+11:13:31.4	52.6	B 21.3 ± 0.04 ± 0.2
B0914+114	"	"	09:17:16.54	+11:13:32.3	44.4	V 19.9 ± 0.01 ± 0.1

The radio positions are from the VLA calibrator manual (B0008-421, B0316+161, B0742+103) and NED (B0407–658, B0554–026, B0904+039, B0914+114). The typical uncertainties in the radio positions are 0.01″ in Declination and 0.001s in Right Ascension. The R_1 factor is the likelihood ratio (see text for details). The optical coordinates of B0914+114 correspond to the galaxy previously – and incorrectly – identified as the counterpart (see notes on individual source). The errors in the magnitudes are divided in photon noise (first error) and calibration (second error). The magnitudes are corrected for Galactic extinction, following Schlegel et al. (1998). B0316+161 magnitudes may be affected by close-by (∼3″) objects.

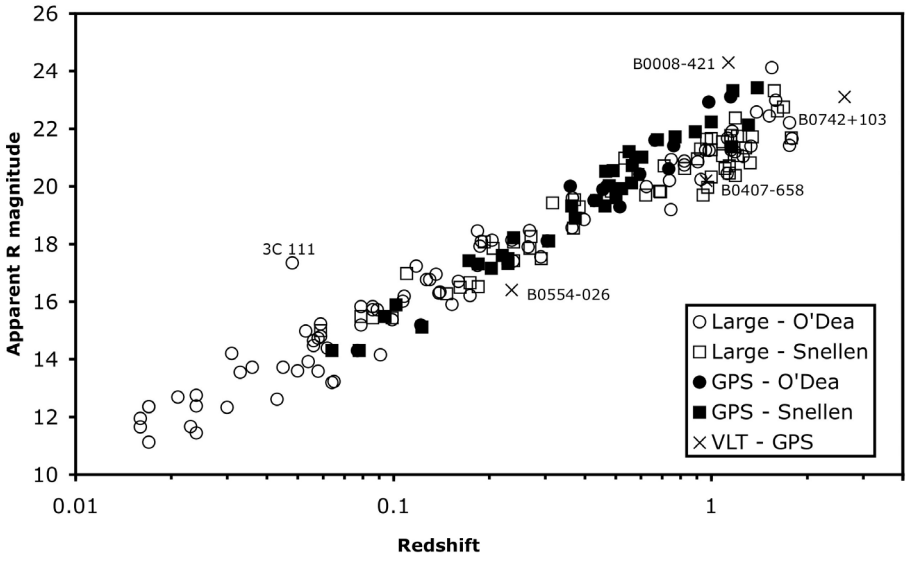

Fig. 1. *R*-band Hubble diagram for GPS and large radio galaxies. Data from O'Dea et al. (1996), Snellen et al. (2002) and our VLT measurements (marked with X). Redshifts of B0742+103 and B0554–026 from Best et al. (2003) and de Vries et al. (2000b). 3C 111 is obscured by the Galactic dark cloud complex Taurus B (e.g., Sguera et al. 2005, and references therein).

3.4. Stellar population synthesis models

GPS radio sources are found to live in passively evolving elliptical galaxies, and have colors consistent with those predicted by stellar synthesis models (e.g., O'Dea et al. 1996; de Vries et al. 1998; Snellen et al. 2002). Most of our objects are identified with *galaxies* and not quasars. Therefore, most of the optical radiation can be associated with stars in the host.

We have compared our redshift and magnitude measurements with the Bruzual & Charlot (2003) stellar population synthesis models. The models have been run using the Chabrier (Chabrier 2003) initial mass function, metallicities $Z = 0.008$, $Z = 0.02$, $Z = 0.05$ and ages (time since the initial starburst) ranging from 5 to 12.5 Gyr. Different star formation histories have been used: instantaneous burst, exponentially declining, and constant star formation. We fitted colors $B - V$ and $V - R$ for the sources where we had color information.

Constant and exponentially declining star formation models seem to be ruled out by our data. The data points and best models disagree by roughly 0.5 to 1 mag.

The optical color data are in better agreement with the passively evolving instantaneous burst models (Fig. 2), consistent with previous works (e.g., de Vries et al. 2000a). Our data seem to favor models with ages of ∼12 Gyr and metallicity 0.008. However, the known degeneracy between metallicities and ages suggests that these results should be viewed with caution. In addition, we note that our HST UV observations suggest that many GPS hosts contain a small contribution from recent star formation (Labiano et al. 2006, 2007, in prep.).

4. Notes on individual sources

B0008–421: following unsuccessful attempts by di Serego-Alighieri et al. (1994), de Vries et al. (1995)

Table 3. Line identifications and redshifts.

Name	ID	Line	Wavelength (Å)	Redshift	Mean	Flux	*FWHM*	Log Power 5 GHz
B0008–421	G	[Ne V] 3425?	7294	1.130	1.130*	0.3	29	26.7
		[O II] 3727?	7940	1.130		0.7	39	
B0316+161	G	[O II] 3727	7102	0.906	0.907	5.4	21	27.6
		[Ne III] 3869	7381	0.908		1.8	32	
		H_β 4861	9277	0.908		4.7	49	
		[O III] 4959	9464	0.908		8.3	35	
		[O III] 5007	9544	0.906		33	51	
B0407–658	G	[Ne V] 3425	6721	0.962	0.962	11	25	27.7
		[O II] 3727	7314	0.962		6.9	29	
		[Ne III] 3869	7595	0.963		2.0	44	
		[Ne III] 3967	7787	0.963		0.7	29	
		H_γ 4102	8048	0.962		0.3	18	
		H_β 4861	9538	0.962		4.4	52	
		[O III] 4959	9731	0.962		43	51	
		[O III] 5007	9823	0.962		16	54	
B0904+039	G	[O II] 3727	6822	0.830	0.830	1.9	17	24.9
		[O III] 4959	9078	0.831		1.8	26	
		[O III] 5007	9162	0.830		4.4	26	
B0914+114	G	Break 4000	4711	0.178	0.178	–	–	–
		Hβ 4861	5690?	0.171?	±0.005	–	–	
		Mgb 5200	6115	0.183		–	–	
		[N II] 6548	7667	0.171		–	–	
		Hα 6563	7772	0.184		–	–	
		[S II] 6716	7952	0.184		–	–	
B1045+019		[O II] 3727	6297	0.689	0.689*	0.4	12	26.6
		H_γ 4102	7327	0.688		0.3	12	
		[He II] 4686	7918	0.689		0.3	29	
PMN J1300–1059	Q?	Mg II 2799	6385	1.283	1.283*	10	125	–
B1433–040	Q	[O II] 3727	6694	0.796	0.795	17	19	26.3
		[Ne III] 3869	6949	0.796		32	54	
		[Ne III] 3967	7122	0.795		10	21	
		H_δ 4102	7355	0.794		23	84	
		H_γ 4341	7790	0.795		76	113	
		H_β 4861	8724	0.795		347	192	
		[O III] 4959	8900	0.795		63	30	
		[O III] 5007	8987	0.795		121	27	

For B1433–040, the redshift is measured with the narrow emission profiles. The * means the redshift estimation is uncertain for that source, see text for details. The *FWHM* listed is the observed *FWHM* corrected for the *FWHM* of the instrumental spectrum. Fluxes in 10^{-16} erg/cm^2/s. A conservative error for z is ±0.001. The B0914+114 results correspond to the unrelated galaxy. It shows emission and absorption lines mixed so the centers are more uncertain than in the other sources (the 1σ error in z is listed below the mean value) and line properties will depend on the stellar population model. The last column lists the radio power in W/Hz of the source for the redshifts listed. The 5 GHz fluxes are from O'Dea (1998) and Wright & Otrupcek (1990).

and Costa (2001), we have now identified the bright radio source B0008–421 with an $R = 24.3$, somewhat diffuse galaxy (Fig. 4). This magnitude is consistent with previous non-detections (which had detection limits down to magnitude 23). We detect a faint object, 0.2″ from the VLBI position. The spectrum is consequently faint and very noisy making it difficult to distinguish emission lines from noise (Fig. 3). Comparison with the GPS Hubble diagram (O'Dea et al. 1996, see Fig. 1) shows that for an apparent R magnitude ∼24, the expected redshift is between 1 and 2. We find two dubious emission lines consistent with this range of redshift: [Ne V]λ3425 and [O II]λ3727 at 7294 Å and 7940 Å, which would correspond to a redshift of $z = 1.130$.

B0316+161: our deep image (Fig. 4) confirms the earlier identification of this well known GPS radio source (also known as CTA21), by Stanghellini et al. (1993). We find a rather compact host, and note that the object seen 8″ NNW of the CTA21 identification in the Stanghellini et al. image is unrelated. The relative faintness of B0316+161, and the proximity of bright objects, may be affecting our measured magnitudes. The spectrum shows a weak continuum with bright [O II] and [O III] lines (Fig. 4). We measure $z = 0.907$ based on five lines.

B0407–658: Stickel et al. (1996) identified the optical counterpart of this radio source as a galaxy. The spectrum (Fig. 3) shows a faint continuum spectrum where we identify nine emission lines at $z = 0.962$. The emission line gas is more extended (3.2″, 25 kpc) along the slit than the stellar continuum. We observe no shift in wavelength along the spatial direction in the spectra. Our resolution (∼18 Å) yields a velocity resolution limit of ∼500 km s^{-1} for the central part of the spectrum. Recent radio spectral data (NED)[2] show no peak around 1 GHz for this source, suggesting a CSS or larger radio source. However, the source is unresolved in ATCA observations (resolution ∼5 × 3″ Morganti et al. 1993).

B0437–454: the spectrum shows a bright continuum but no emission or absorption lines. Updated radio data indicate that the radio spectrum of B0437–454 is only marginally peaked. In addition, pronounced variability was reported: 0.6 Jy vs. 1.4 Jy

[2] NASA/IPAC Extragalactic Database.

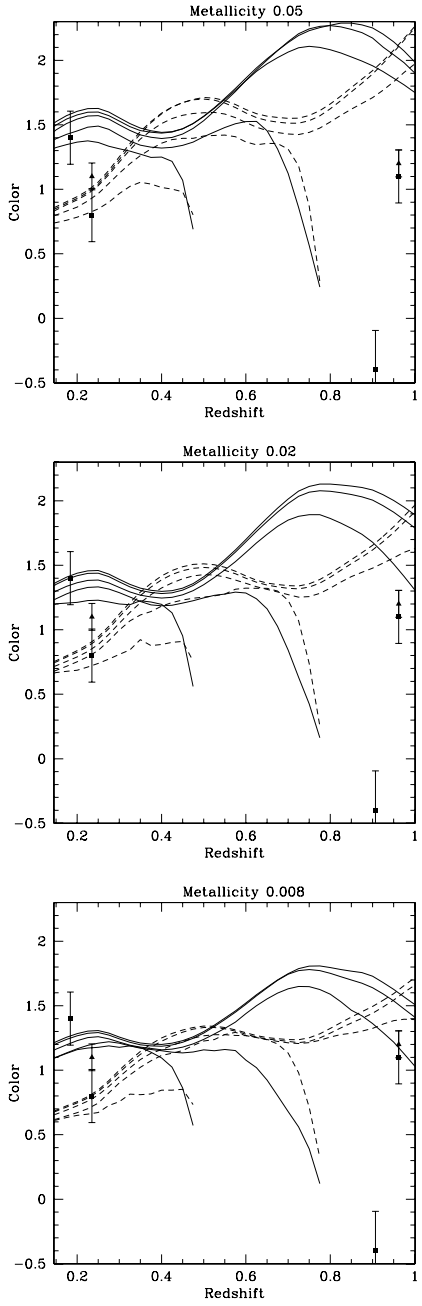

Fig. 2. Instantaneous, single burst stellar population synthesis models (lines) and observational colors (points) for our data. Squares and solid lines represent $B-V$, triangles and dashed lines represent $V-R$. There are five ages represented for each color: 5.0, 6.8, 9.3, 11.5 and 12.5 Gyr. The age of the population increases from bottom to top. The discrepant data point corresponds to B0316+161 (at $z = 0.907$). However, the measured color of B0316+161 may be affected by bright nearby objects.

at 5 GHz (e.g., Wright et al. 1994; Wright & Otrupcek 1990). Also, given the identification with an optical point source, we conclude that the object is probably a BL Lac object and should be removed from the GPS list.

B0554–026: we confirm the identification of de Vries et al. (2000b) ($z = 0.283$) of this galaxy. We find a rather bright ($B = 18.3$, $V = 17.5$) and extended source (~5″). We obtain $R = 16.4$ but this band may be affected by calibration problems (see Sect. 3.2).

B0742+103: neither Stickel et al. (1996) nor de Vries et al. (1995) were able to identify the host of this relatively bright radio source. Our UT1 image (Fig. 4), which unambiguously identifies the source with a compact host galaxy, indicates that the tentative identifications by Fugmann et al. (1988) and de Vries et al. (2000b) were correct: we establish $R = 23.1$. We obtained long slit spectra of this source both in the January and the December run. Both observations show a faint spectrum and features which could be lines. However, none of these features are present in both spectra. Best et al. (2003) measure 2.624 ± 0.003 based on Ly α, C IV, He II and C III] between 4400 and 6920 Å. We detect a faint (slightly brighter than noise) emission at 6922 Å which could be the Best et al. (2003) C III]. Having only one emission feature, we cannot get an independent redshift measurement. If their redshift is correct, using the 5 GHz flux density from O'Dea (1998), the source would have a radio power of 2.1×10^{28} W/Hz.

B0904+039: the deep UT1 image (Fig. 4) reinforces the earlier identification of this GPS radio source (de Vries et al. 2000b, $I = 22.5$) with a faint host ($V = 24.9$) in a group of faint galaxies. The spectrum shows a weak continuum (Fig. 3). We measure $z = 0.830$ based on the [O II] and [O III] lines.

B0914+114: our B and V band images show an empty field at the accurate FIRST survey radio coordinates (Fig. 4). Based on uncertain WSRT coordinates, Stanghellini et al. (1993) suggested that the disk galaxy ~6″ south of the current radio position could be the host of the radio source. Thus, this disk galaxy is not the optical counterpart of the GPS source. We obtained a spectrum of the disk galaxy, which shows a faint stellar dominated continuum (Fig. 3). We observe narrow Hα and Hβ in emission on top of a broad absorption which also may be affecting [N II] and [S II] emission. Averaging the redshifts of all the observed features, we obtain $z = 0.178$. The Hα emission at 7772 Å had been detected before (de Vries et al. 2000b).

B1045+019: the weak continuum and noisy spectrum makes it difficult to distinguish real emission lines from noise. We only find one – dubious – possibility for redshift ($z = 0.689$). If this redshift is correct, we are not detecting Hβ and [O III] 5007 (at 8200 and 8550 Å respectively). Radio observations were discussed in de Vries et al. (2000b) suggesting that this radio source may not be a GPS.

PMN J1300–1059: this source is from a list of candidate GPS sources found by comparing VLA NVSS and WSRT WISH survey data. We find one emission line at 6385 Å. The emission may consist of a narrow (~80 Å) and a broad (~200 Å) component but the edge of the chip is too close to deblend it accurately. This line could be Mg II λ 2799 at $z = 1.283$, and in that case the [O II] doublet at 3727 Å is not detected. If it were C IVλ1549, we would expect C III]λ1909 at 7826 Å. The relatively bright continuum suggests a QSO, which would be consistent with broad Mg II.

B1433–040: de Vries et al. (2000b) already drew attention to the fact that the GPS source B1433–040 should not be identified with the considerably brighter radio source 4C –04.51. The optical spectrum shows a very strong continuum with broad (~200 Å) and narrow (~30 Å) emission lines (Fig. 3). The spectral shape and presence of bright broad lines is consistent with a QSO. We observe a strong asymmetry in the broad emission. The asymmetry index (AI20, Heckman et al. 1981) is defined as (WL20–WR20)/(WL20+WR20), where WL20 and WR20 are the half width of the line to the left (WL20) and right (WR20) at the 20% intensity level. We measure AI20 ~ 0.35, towards the red, for Hβ (and Hγ), which is large, but not unusual. This asymmetry can be explained by inflow or outflow of gas, together with a line opacity (or scatter) cloud which blocks the

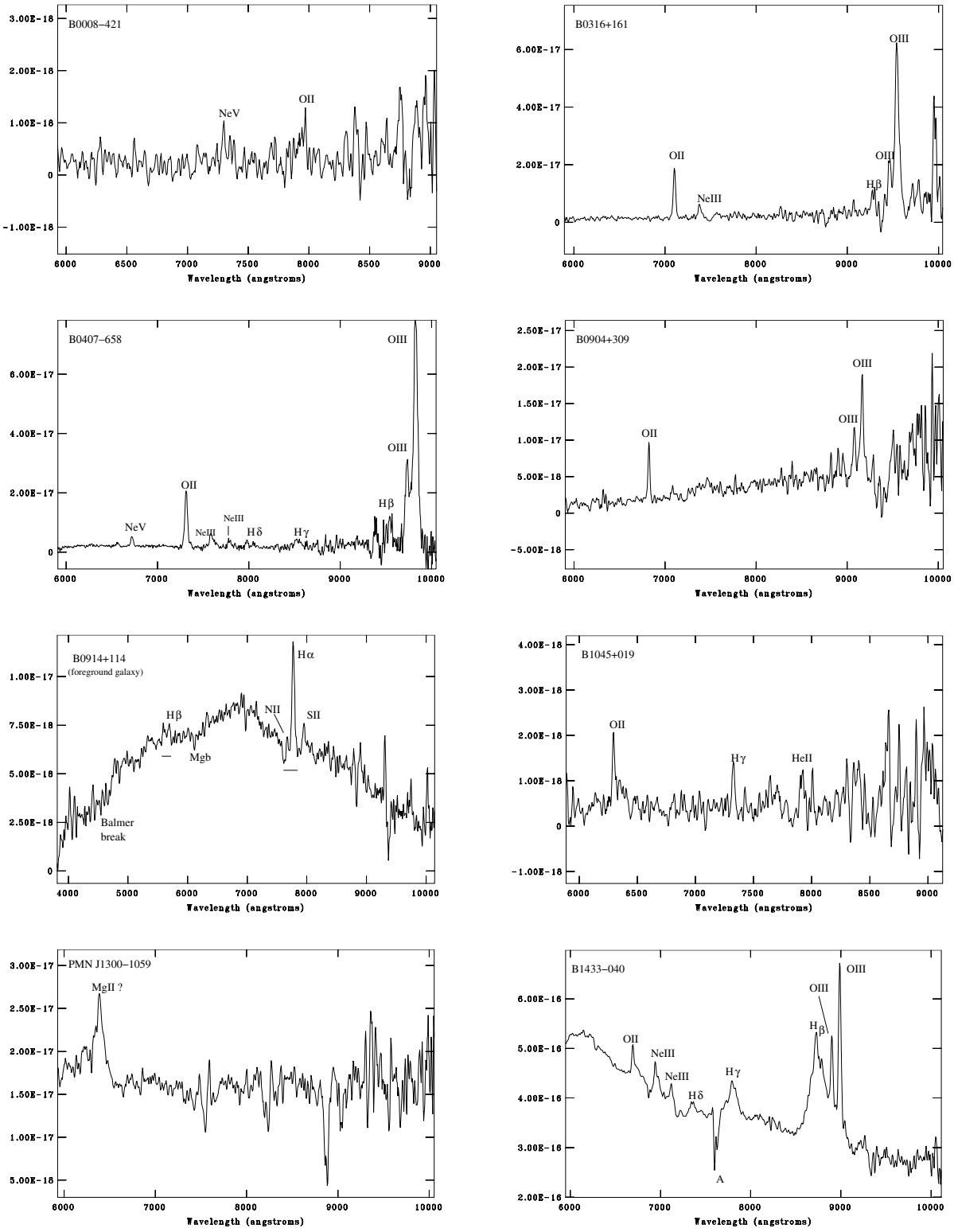

Fig. 3. Spectra of the sources with identified emission lines. Flux is in erg cm^{-2} s^{-1} Å^{-1}. B0914+114: the spectrum corresponds to the previous – incorrect – identification (see text for details). The horizontal lines show an estimation of the possible *FWHM* of the absorption hydrogen lines.

emission at one side of the AGN (e.g., Whittle 1985, and references therein). The optical spectrum of this radio source displays hydrogen emission lines of striking velocity width: we measure 28 000 km s^{-1} FWZI for Hβ, and note in addition its double-peaked nature. The radio spectrum has a relatively broad peak around 1 GHz (e.g., Spoelstra et al. 1985). However, more observations, especially at frequencies $\lesssim$1 GHz, are needed. There seems to be some variability in the 408 MHz and ~1.4 GHz (Large et al. 1981; Wright & Otrupcek 1990; White & Becker 1992) observed flux densities. Given the unresolved optical host, we suggest that the optical counterpart of B1433–040 is a quasar at $z = 0.796$.

B1601–222: featureless, very noisy spectrum with a moderately bright continuum. Snellen et al. (2002) measure $z = 0.141$ based on the absorption features: *G*-band 4300, Hβ 4861, Mg b 5169 and Na D 5899, which correspond to ~4900–6800 Å.

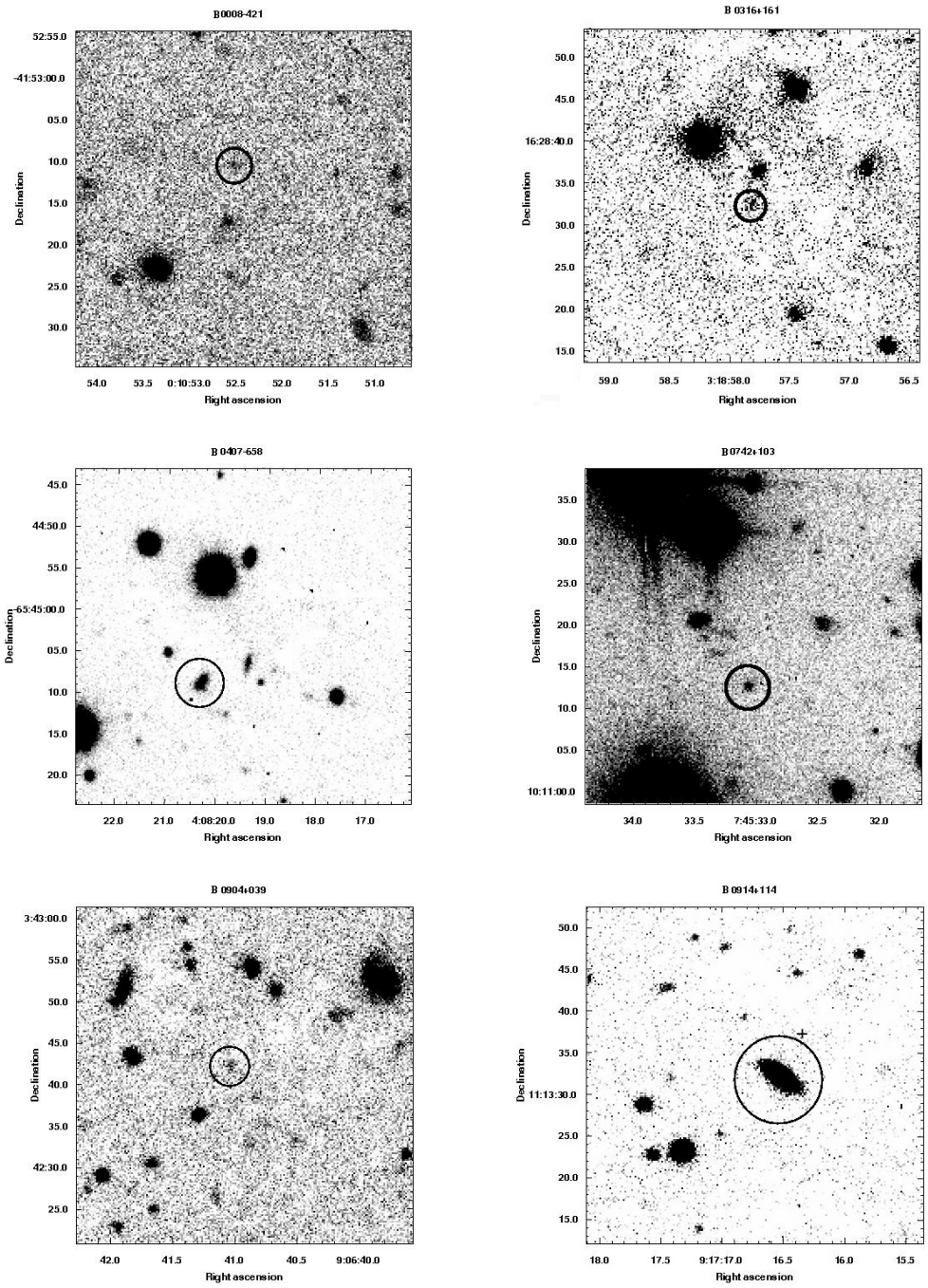

Fig. 4. Finding charts for the identified sources. The images correspond to the band of our VLT observations were sources were brighter. The radio position of 0914+114 is 6″ north of the observed galaxy (circled) which was previously – and incorrectly – identified as the optical counterpart (see text). The radio position is marked with a cross.

We covered the range between 5700 and 9200 Å and observe no features. However, their spectrum has higher wavelength resolution and longer exposure time (2700 s).

B1648+015: featureless with a not very bright continuum. Stickel et al. (1996) identifies this source as a quasar. The radio spectrum shows variability so it is probably either a flat spectrum quasar or a BL Lac object.

5. Master list

We have updated the O'Dea et al. (1991) GPS sources master list with new available data (Table 4). This new list consists of those radio sources with intrinsic turnover frequency between 0.4 and 5 GHz (GPS) or higher (High Frequency Peakers, HFP). For sources with unknown redshift, we have extended the selection down to 0.3 GHz. We expect this list to be useful for workers in the field of radio galaxies and quasars in general, and compact radio sources and AGN hosts in particular. The list is furthermore electronically available via URL `http://www.damir.iem.csic.es/extragalactic/people/labiano/` and `http://www.cis.rit.edu/~cposps/`.

6. Summary

We presented VLT deep optical imaging and spectroscopy targeting the host galaxies of GPS radio sources. The sample was

comprised of unidentified objects from the master list of O'Dea et al. (1991), updated by de Vries et al. (1997).

We have found new optical counterparts (down to magnitudes ∼25) of GPS sources B0008–421 and B0742+103 and confirmed previous identifications of GPS sources: B0316+161, B0407–658, B0554–026, B0904+039. With new radio observations from the literature, we find that the radio spectra of B0407–658, B0437–454 and B1648+015 suggest that these sources are not GPS. However, high resolution radio observations are needed to confirm it. We do not detect the optical counterpart of B0914+114 and suggest that previous identification corresponds to an unrelated galaxy (at $z = 0.178$), 6″ South of the current radio position.

We measure new redshifts for B0316+161, B0407–658, B0904+039, B0914+114 (unrelated galaxy) and B1433–040, and propose uncertain redshifts for B0008–421, B1045+019, PMN J1300–1059. The following sources remain with undetermined redshift: B0437–454, B0914+114 and B1648+015. We cannot confirm previous redshifts of: B0742+103, B1601–222. Our magnitudes seem to be consistent with previous measurements of GPS counterparts.

Stellar population synthesis models are inconsistent with constant or exponentially declining star formation in the host. The data generally agree with single instantaneous burst models in a passively evolving host, but do not yield useful information on age or metallicity.

Acknowledgements. A.L. wishes to thank Prof. Dr. R. F. Peletier (Kapteyn Astronomical Institute) for useful scientific discussions. This paper is based on observations made with ESO Telescopes at Paranal Observatory under Programmes 64.P–0482(A) and 68.B–0044(A)). This research has made use of NASA's Astrophysics Data System Bibliographic Services and of the NASA/IPAC Extragalactic Database (NED) which is operated by the Jet Propulsion Laboratory, California Institute of Technology, under contract with the National Aeronautics and Space Administration. WDVs work was performed under the auspices of the US Department of Energy, National Nuclear Security Administration by the University of California, Lawrence Livermore National Laboratory under contract No. W-7405-Eng-48.

References

Appenzeller, I., Fricke, K., Furtig, W., et al. 1998, The Messenger, 94, 1
Augusto, P., Gonzalez-Serrano, J. I., Perez-Fournon, I., & Wilkinson, P. N. 2006, MNRAS, 368, 1411
Beasley, A. J., Gordon, D., Peck, A. B., et al. 2002, ApJS, 141, 13
Becker, R. H., White, R. L., & Edwards, A. L. 1991, ApJS, 75, 1
Begelman, M. C. 1996, in Cygnus A – Study of a Radio Galaxy, 209
Best, P. N., Peacock, J. A., Brookes, M. H., et al. 2003, MNRAS, 346, 1021
Bruzual, G., & Charlot, S. 2003, MNRAS, 344, 1000
Chabrier, G. 2003, PASP, 115, 763
Condon, J. J., Cotton, W. D., Greisen, E. W., et al. 1998, AJ, 115, 1693
Costa, E. 2001, A&A, 367, 719
Dallacasa, D., Stanghellini, C., Centonza, M., & Fanti, R. 2000, A&A, 363, 887
De Breuck, C., Tang, Y., de Bruyn, A. G., Röttgering, H., & van Breugel, W. 2002, A&A, 394, 59
de Ruiter, H. R., Arp, H. C., & Willis, A. G. 1977, A&AS, 28, 211
de Vries, W. H., Barthel, P. D., & Hes, R. 1995, A&AS, 114, 259
de Vries, W. H., Barthel, P. D., & O'Dea, C. P. 1997, A&A, 321, 105
de Vries, W. H., O'Dea, C. P., Baum, S. A., et al. 1998, ApJ, 503, 156
de Vries, W. H., O'Dea, C. P., Barthel, P. D., et al. 2000a, AJ, 120, 2300
de Vries, W. H., O'Dea, C. P., Barthel, P. D., & Thompson, D. J. 2000b, A&AS, 143, 181
De Young, D. S. 1997, ApJ, 490, L55
di Serego-Alighieri, S., Danziger, I. J., Morganti, R., & Tadhunter, C. N. 1994, MNRAS, 269, 998
Edwards, P. G., & Tingay, S. J. 2004, A&A, 424, 91
Fanti, C., Fanti, R., Dallacasa, D., et al. 1995, A&A, 302, 317
Fugmann, W., Meisenheimer, K., & Roeser, H.-J. 1988, A&AS, 75, 173
Griffith, M. R., Wright, A. E., Burke, B. F., & Ekers, R. D. 1994, ApJS, 90, 179
Heckman, T. M., Miley, G. K., van Breugel, W. J. M., & Butcher, H. R. 1981, ApJ, 247, 403
Kaiser, C. R., & Alexander, P. 1997, MNRAS, 286, 215
Kaiser, C. R., Dennett-Thorpe, J., & Alexander, P. 1997, MNRAS, 292, 723
Kent, S. M. 1985, PASP, 97, 165
Kuehr, H., Witzel, A., Pauliny-Toth, I. I. K., & Nauber, U. 1981, A&AS, 45, 367
Labiano, A., O'Dea, C. P., Barthel, P. D., de Vries, W. H., & Baum, S. A. 2006, New A Rev., 50, 776
Labiano, A., O'Dea, C. P., Barthel, P. D., de Vries, W. H., & Baum, S. A. 2007, in prep.
Landolt, A. U. 1992, AJ, 104, 372
Large, M. I., Mills, B. Y., Little, A. G., Crawford, D. F., & Sutton, J. M. 1981, MNRAS, 194, 693
Marcha, M. J. M., Browne, I. W. A., Impey, C. D., & Smith, P. S. 1996, MNRAS, 281, 425
McLean, B., Hawkins, C., Spagna, A., et al. 1998, in New Horizons from Multi-Wavelength Sky Surveys, ed. B. J. McLean, D. A. Golombek, J. J. E. Hayes, & H. E. Payne, IAU Symp., 179, 431
Morganti, R., Killeen, N. E. B., & Tadhunter, C. N. 1993, MNRAS, 263, 1023
Morganti, R., Tadhunter, C. N., Dickson, R., & Shaw, M. 1997, A&A, 326, 130
O'Dea, C. P. 1998, PASP, 110, 493
O'Dea, C. P., & Baum, S. A. 1997, AJ, 113, 148
O'Dea, C. P., Baum, S. A., & Stanghellini, C. 1991, ApJ, 380, 66
O'Dea, C. P., Stanghellini, C., Baum, S. A., & Charlot, S. 1996, ApJ, 470, 806
Readhead, A. C. S., Taylor, G. B., Pearson, T. J., & Wilkinson, P. N. 1996, ApJ, 460, 634
Schlegel, D. J., Finkbeiner, D. P., & Davis, M. 1998, ApJ, 500, 525
Sguera, V., Bassani, L., Malizia, A., et al. 2005, A&A, 430, 107
Snellen, I. A. G., Bremer, M. N., Schilizzi, R. T., Miley, G. K., & van Ojik, R. 1996, MNRAS, 279, 1294
Snellen, I. A. G., Schilizzi, R. T., de Bruyn, A. G., et al. 1998, A&AS, 131, 435
Snellen, I. A. G., Schilizzi, R. T., Bremer, M. N., et al. 1999, MNRAS, 307, 149
Snellen, I. A. G., Schilizzi, R. T., Miley, G. K., et al. 2000, MNRAS, 319, 445
Snellen, I. A. G., Lehnert, M. D., Bremer, M. N., & Schilizzi, R. T. 2002, MNRAS, 337, 981
Snellen, I. A. G., Mack, K.-H., Schilizzi, R. T., & Tschager, W. 2004, MNRAS, 348, 227
Spergel, D. N., Verde, L., Peiris, H. V., et al. 2003, ApJS, 148, 175
Spoelstra, T. A. T., Patnaik, A. R., & Gopal-Krishna. 1985, A&A, 152, 38
Stanghellini, C., O'Dea, C. P., Baum, S. A., & Laurikainen, E. 1993, ApJS, 88, 1
Stickel, M., Rieke, G. H., Kuehr, H., & Rieke, M. J. 1996, ApJ, 468, 556
Tadhunter, C. N., Morganti, R., di Serego-Alighieri, S., Fosbury, R. A. E., & Danziger, I. J. 1993, MNRAS, 263, 999
Tinti, S., Dallacasa, D., de Zotti, G., Celotti, A., & Stanghellini, C. 2005, A&A, 432, 31
Torniainen, I., Tornikoski, M., Teräsranta, H., Aller, M. F., & Aller, H. D. 2005, A&A, 435, 839
Urry, C. M., & Padovani, P. 1995, PASP, 107, 803
White, R. L., & Becker, R. H. 1992, ApJS, 79, 331
Whittle, M. 1985, MNRAS, 213, 1
Wright, A., & Otrupcek, R. 1990, in PKS Catalog (1990), 0
Wright, A. E., Griffith, M. R., Burke, B. F., & Ekers, R. D. 1994, ApJS, 91, 111
Xiang, L., Reynolds, C., Strom, R. G., & Dallacasa, D. 2006, A&A, 454, 729
Xu, W., Lawrence, C. R., Readhead, A. C. S., & Pearson, T. J. 1994, AJ, 108, 395
Xiang, L., Stanghellini, C., Dallacasa, D., & Haiyan, Z. 2002, A&A, 385, 768
Zensus, J. A., Ros, E., Kellermann, K. I., et al. 2002, AJ, 124, 662

Online Material

Table 4. Master list.

(1) Name	(2) Other	(3) GPS/HFP	(4) ID	(5) Redshift	(6) Refs.	(7) ν_{peak} (GHz)	(8) Ref.	(9) $\nu_{peakint}$ (GHz)	(10) Flux (Jy)	(11) Frequency (GHz)	(12) Ref.
000319+212944	0000+212	HFP	G	0.4	5	6.2	6		0.265	5	6
000346+480703	0001+478	GPS			7	1	N	1	0.197	4.85	9
000520+052410	0002+051	HFP	Q	1.887	5	4.9	6	14.1	0.229	5	6
001052–415310	0008–42	GPS	G		2	0.5	N	0.5	1.12	5	10
002127+731241	0018+729	GPS	G	0.821	8, 29	1	N	1.8	0.393	4.85	9
002225+001456	4C+00.02	GPS	G	0.305	29	0.7	11	0.9	1.1	5	11
002442–420203	0022–423	GPS	Q	0.937	2	1.6	0	3.1	1.7	5	0
002914+345632	0026+346	GPS	G	0.517	1, 12	1	N	1.5	1.32	4.85	9
003732+080813	0034+078	HFP	G?	>1.8	5	4.9	6	>13.7	0.292	5	6
004204+232001	0039+230	GPS			1	1?	N	1?	1.65	4.85	9
010813–120050	0105–122	GPS	G		4	1	4	1	0.52	2.7	4
011137+390628	0108+388	HFP	G	0.66847	1, 29	4	11	6.7	1.26	5	11
011638+242253	0113+241	GPS			5	4.9	6	4.9	0.243	5	6
011935+321050	4C+31.04	GPS	G	0.06	7, 13	0.4	N	0.4	1.59	4.85	9
014658+211024	0144+209	GPS			1	1.3?	N	1.3?	0.598	4.85	9
015310–331025	0150–334	GPS	Q	0.61	3	1.5	3	2.4	0.88	4.8	3
020434+090349	0201+088	GPS			7	∼2	N	∼2	0.774	4.85	9
020346+113445	0201+113	HFP	Q	3.639	1, 29	∼4	N	17.3	0.742	4.85	9
020643–302458	0204–306	GPS	G		4	0.5	4	0.5	0.58	2.7	4
021010–221336	0207–224	GPS	G		4	1.5	4	1.5	0.85	2.7	4
021044+041934	0208+040	GPS			4	0.4	4	0.4	0.56	2.7	4
024008–230915	0237–233	GPS	Q	2.223	11, 1	1	11	3.2	3.34	5	11
024235–213226	0240–217	GPS	G	0.314	4	1	4	1.3	0.97	2.7	4
025134+431515	0248+430	HFP	Q	1.32	1, 29	7	29	16.2	1.24	5	30
031857+162833	4C+16.09	GPS	Q		11	0.8	11	0.8	2.89	5	11
032153+122113	0319+121	GPS	Q	2.662	1	0.4	11	1.5	1.1	5	11
032320+053411	4C+05.14	GPS	G	0.1785	4, 14	0.4	4	0.5	1.6	2.7	4
035721+231953	0354+231	HFP	Q		5	>22	6		0.56	5	6
040121–292126	0359–294	GPS	G		4	0.4	4	0.4	0.58	2.7	4
041046+765645	4C+76.03	GPS	G	0.5985	1	0.6	0	1	2.82	5	0
040757–275705	0405–280	GPS	G		4	1.5	4	1.5	0.93	2.7	4
040734–392447	0405–395	GPS	G		4	0.4	4	0.4	0.52	2.7	4
042214–384452	0420–388	GPS	Q	3.11	1	?	N	?	0.13	4.85	26
042746+413301	0424+414	GPS			7,	∼2	N	∼2	0.723	4.85	9
043103+203734	0428+205	GPS	G	0.219	1, 29	1.1	11	1.3	2.38	5	11
043354–022956	4C –02.17	GPS	G		4	0.4	4	0.4	1.04	2.7	4
043701–184448	0434–188	HFP	Q	2.702	3	4.5	3	16.7	0.95	4.8	3
044133–334003	0439–337	GPS			4	1.5	4	1.5	0.88	2.7	4
045720–084905	0454–088	GPS	G		4	0.4	4	0.4	0.58	2.7	4
045952+022931	0457+024	HFP	Q	2.384	1, 29	2.1	11	7.1	1.57	5	11
050321+020305	0500+019	GPS	Q	0.58457	2, 7	1.8	11	2.9	1.89	5	11
051002+180042	0507+179	GPS	Q	0.3	29	1.4	0	1.8	0.73	5	0
053008–250330	0528–250	HFP	Q	2.813	1, 29	2.7	N	10.3	1.16	5	10
055652–024105	0554–026	GPS	G	0.235	18	1	0	1.2	0.29	5	0
062518+444002	0621+446	HFP			5	14	6		0.442	5	6
063802+593322	0633+595	HFP			5	12.9	6		0.591	5	6
064204+675836	0636+680	HFP	Q	3.18	1	3.7	6	15.5	0.474	5	6
064425–345942	0642–349	HFP	Q	2.165	3	3.3	3	10.5	0.85	4.8	3
064632+445117	0642+449	HFP	Q	3.396	5	15.5	6	68.1	1.896	5	6
065031+600143	0646+600	HFP	Q	0.455	1, 5	6.8	6	9.9	1.236	5	6
070648+464756	0703+468	GPS	Q?		7	0.5	0	0.5	0.62	4.85	9
071338+434917	0710+439	GPS	G	0.518	1, 11	1.9	11	2.9	1.68	5	11

Table 4. continued.

(1) Name	(2) Other	(3) GPS/HFP	(4) ID	(5) Redshift	(6) Refs.	(7) ν_{peak} (GHz)	(8) Ref.	(9) $\nu_{peakint}$ (GHz)	(10) Flux (Jy)	(11) Frequency (GHz)	(12) Ref.
071424+353439	0711+356	GPS	Q	1.62	1, 29	1.4	N	3.7	0.89	4.85	9
071509+452555	0711+453	GPS	G	0.042	16	3.8	16	4.0	0.074	1.4	16
072550+391725	4C+39.17	GPS	G		7	0.5?	N	0.5?	0.23	4.85	9
073328+560541	0729+562	GPS	G	0.104	16	0.46	16	0.5	0.394	1.4	16
073934+495438	0735+500	GPS	G	0.054	16	0.95	16	1	0.107	1.4	16
074533+101112	0742+103	HFP	G	2.624	17	2.7	11	9.8	3.46	5	11
074554–004418	0743–006	HFP	Q	0.994	17	5.8	11	11.6	2.05	5	11
075415+532456	0750+535	GPS			7	1.4	N	1.4	0.29	4.85	9
080454+433537	0801+437	GPS	Q	0.123	16	1.5	16	1.7	0.36	1.4	16
080538+210651	0802+212	GPS	G		1	1.4	N	1.4	0.56	4.85	9
083139+460800	0828+461	GPS	G	0.127	16	2.2	16	2.5	0.131	1.4	16
090040–280820	0858–279	GPS	Q	2.16	1, 29	1.4	29	4.4	1.38	5	27
090615+463618	0902+468	GPS	G	0.085	16	0.68	16	0.7	0.314	1.4	16
090641+034242	0904+039	GPS	G		1	∼0.6	N	∼0.6	0.208	4.85	9
091335+145420	0910+151	GPS			4	0.6	4	0.6	0.54	2.7	4
091716+111336	0914+114	GPS			11	0.4?	N	0.4?	0.13	5	0
093609+331308	0933+332	GPS	G	0.076	16	2.2	16	2.4	0.055	1.4	16
094336–081931	0941–080	GPS	G	0.228	11, 1	0.5	11	0.6	1.11	5	11
103507+562847	1031+567	GPS	Q	0.459	29	1.3	11	1.9	1.28	5	11
104437–271218	1042–269	GPS			4	1.5	4	1.5	0.55	2.7	4
105715+001203	1054+004	GPS			4	0.4	4	0.4	0.58	2.7	4
105731+405646	NGC 3468	GPS	G	0.008	16	1.25	16	1.3	0.047	1.4	16
110323+220337	1100+223	GPS			1	2.7	N	2.7	0.58	4.85	9
110946+104343	1107+109	GPS	G		4	0.5	4	0.5	0.8	2.7	4
111000–185848	1107–187	GPS	G	0.497	4	1	4	1.5	0.65	2.7	4
111120+195536	1108+201	GPS	G	0.299	7	1	N	1.3	0.64	4.85	9
112027+142054	4C+14.41	GPS	G	0.362	11	0.5	11	0.7	1	5	11
112125–055356	1118–056	GPS			29	0.9	29		0.57	5	27
112256–274248	1120–274	GPS			4	1.4	4	1.4	0.74	2.7	4
113007–144927	1127–145	GPS	Q	1.187	11	1	11	2.2	3.82	5	11
113513–002119	4C–00.45	GPS	Q		4	0.4	4	0.4	0.76	2.7	4
113555+425844	1133+432	GPS			15	1.0	29	∼1	0.42	5	15
114608–244731	1143–245	GPS	Q	1.95	11	2.2	11	6.5	1.4	5	11
120321+041417	1200+045	GPS	G	1.21177	4	0.4	4	0.9	0.52	2.7	4
122758+363511	1225+36	GPS	Q	1.973	1, 24	1.2	11	3.6	0.77	5	11
124823–195918	1245–197	GPS	Q	1.275	1, 29	0.5	11	1.1	2.34	5	11
130041–105908	1258-104	GPS	Q?	1.283?	19.28	?	N	?	0.07	4.85	25
131338+693909	1312+695	GPS			1	?	N	?	0.26	4.85	9
131739+411545	1315+415	GPS	G	0.066	16	2.3	16	2.5	0.249	1.4	16
132616+315409	4C+32.44	GPS	G	0.369	29	0.5	11	0.7	2.39	5	11
132513+395552	1322+401	GPS	G	0.074	16	1.9	16	2	0.056	1.4	16
133522+454238	1333+459	HFP		2.45	29, 5	5	29	17	0.79	5	5
133525+584400	4C +58.26	GPS			5	4.9	6	4.9	0.723	5	6
134551–301504	1343–300	GPS			4	0.4	4	0.4	0.56	2.7	4
134035+444817	1338+450	GPS	G	0.065	16	2.3	16	2.4	0.082	1.4	16
134733+121724	4C+12.50	GPS	G	0.12174	11, 1	0.4	11	0.4	3.05	5	11
135014–220441	1347–218	GPS	G		4	0.4	4	0.4	0.72	2.7	4
135230+023247	1349+027	GPS	Q		4	0.4	4	0.4	0.78	2.7	4
135256+110707	4C+11.46	GPS			4	0.4	4	0.4	1.04	2.7	4
135706–174402	1354–174	GPS	Q	3.147	1, 29	1.2	N	5	0.97	5	27
140028+621038	4C+62.22	GPS	G	0.431	11, 7	0.5	11	0.7	1.8	5	11
140700+282714	OQ208	GPS	G	0.0769	11, 5	4.2	11	4.5	2.69	5	11
141236+133438	1410+138	GPS			5	4.2	6	4.2	0.33	5	6

Table 4. continued.

(1) Name	(2) Other	(3) GPS/HFP	(4) ID	(5) Redshift	(6) Refs.	(7) ν_{peak} (GHz)	(8) Ref.	(9) $\nu_{peakint}$ (GHz)	(10) Flux (Jy)	(11) Frequency (GHz)	(12) Ref.
142438+225601	1422+231	HFP	Q	3.626	5	4.0	6	18.5	0.61	5	6
143009+104328	1427+109	HFP	Q	1.71	5	4.9	6	13.3	0.91	5	6
143539–041455	1433–04	GPS	G	0.795	11	0.6	N	1.1	0.2	5	0
144516+095836	OQ172	GPS	Q	3.535	11	0.9	11	4.1	1.2	5	11
144516+095836	1444–339	GPS	G		4	0.5	4	0.5	0.5	2.7	4
150506+032630	1502+036	HFP	Q	0.411	5	6.2	6	8.8	0.93	5	6
150603–091912	1503–091	GPS	G		4	0.6	4	0.6	0.87	2.7	4
151141+051809	1509+054	HFP	G	0.084	5	11.0	6	11.9	0.54	5	6
152114+043022	4C+04.51	GPS	Q	1.296	29	0.8	11	1.8	1.09	5	11
152237–273010	1519–273	HFP	Q	1.294	29, 3	5.8	3	6.9	1.74	4.8	3
152642+665054	1526+670	HFP	Q	3.02	5	5.8	6	23.3	0.41	5	6
154301–075707	1540–077	GPS	G	0.172	4	0.4	4	0.5	1.21	2.7	4
154609+002624	1543+005	GPS	G	0.556	18, 4	1.2	0	1.9	0.84	5	0
154812–121331	1545–120	GPS	G	0.883	4	0.4	4	0.8	1.45	2.7	4
155614–062235	4C–06.43	GPS	G		4	0.4	4	0.4	0.77	2.7	4
160000–003723	1557–004	GPS			4	1	4	1	0.54	2.7	4
160207+332653	1600+335	GPS	G	1.1	11, 23	2.4	11	5	2.67	5	11
160631+312710	1604+315	GPS	G	1.5p	1, 31		1.5	29	0.08	4.8	9
160913+264129	CTD93	GPS	G	0.473	1, 29	1.1	11	1.6	1.73	5	11
161637+045932	1614+051	HFP	Q	3.197	1, 6	4.1	6	17.2	0.89	5	6
162418–680913	1619–680	GPS	Q	1.36	3	3.1	3	7.3	1.69	4.8	3
162304+662401	1622+665	HFP	G	0.203	5	5.1	6	6.1	0.3	5	6
164047+122002	4C+12.6	GPS	G	1.152	4	0.4	4	0.9	1.48	2.7	4
164558+633011	1645+635	HFP	Q	2.379	5	>22	6	>74.3	0.51	5	6
164831+024248	4C+02.43	GPS			4	0.4	4	0.4	0.61	2.7	4
165103+012923	1648+015	GPS	Q	0.4	0	1.5	0	2.1	1.03	5	0
165844–073918	1656–075	GPS			3	4.8	3	4.8	1.32	4.8	3
172340–650036	1718–649	GPS	G	0.014	0	4	0	4.1	4.32	5	0
172657–642753	1722–644	GPS			3	1.1	3	1.1	1.26	4.8	3
173458+092657	1732+094	GPS	G	0.61p	7, 4	2.8	0	4.5	0.86	5	0
173549+504911	1734+508	HFP	G?		5	5.9	6		0.97	5	6
174425–514444	1740–517	GPS	G		2	1?	N	1?	3.9	5	27
175301+275059	1751+278	GPS	G	0.86p	1, 15	0.66?	N	1.2	0.27	5	15
171854+544148	1753+544	GPS		0.147	16	0.48	16	0.6	0.33	1.4	16
180356+034108	1801+036	GPS	G		7	?	N	?	0.25	4.85	9
181944+670847	1819+671	GPS	G	0.22	7, 21	~0.5	N	0.6	0.15	4.85	9
182632+270808	1824+271	GPS	G?		15, 29	1?	N	1?	0.115	5	15
183728–710844	1831–711	HFP	Q	1.356	3	8.2	3	19.3	2.39	4.8	3
184057+390046	1839+389	HFP	Q	3.095	5	4.5	6	18.4	0.203	5	6
184103+671849	1841+673	GPS	G	0.47	0	2?	N	2.9?	0.16	5	9
184535+354116	1843+356	GPS	Q	0.764	1, 7	2	0	3.5	0.82	5	0
185027+282514	1848+283	HFP	Q	2.56	1, 5	8.3	6	29.5	1.246	5	6
185527+374257	1853+376	HFP	G	0.5	5	4.5	6	6.8	0.36	5	6
193925–634246	1934–638	GPS	G	0.183	2, 1	1.4	0	1.7	6.5	5	0
194553+705550	1946+708	GPS	G	0.101	7, 21	~0.6	N	0.7	0.64	4.85	9
200324–325147	2000–330	HFP	Q	3.773	1	5	N	23.9	1.2	5	27
201114–064403	2008–068	GPS	G	0.547	4, 29	1.4	11	2.2	1.34	5	11
202135+051505	2019+050	GPS	Q		5	3.7	6	3.7	0.477	5	6
202456+171814	2022+171	HFP	G	0.9	5	14.5	6		0.57	5	6
205252+363535	2050+364	GPS	G	0.354	1, 22	1.2	N	1.6	3.4	4.85	9
205828+054251	4C+05.78	GPS	G	1.381	4	0.4	4	1	0.65	2.7	4
212339–011234	2121–014	GPS	Q	1.158	20	0.5	0	1.1	0.32	5	0
212912–153841	2126–158	GPS	Q	3.27	1, 11	4.1	11	17.5	1.17	5	11

Table 4. continued.

(1) Name	(2) Other	(3) GPS/HFP	(4) ID	(5) Redshift	(6) Refs.	(7) ν_{peak} (GHz)	(8) Ref.	(9) $\nu_{peakint}$ (GHz)	(10) Flux (Jy)	(11) Frequency (GHz)	(12) Ref.
213032+050217	2128+048	GPS	G	0.99	11, 4	0.7	11	1.4	2.02	5	11
215203–780707	2146–783	GPS	Q		3	4.3	3	4.3	1.15	4.8	3
215137+055213	2149+056	GPS	G	0.74	29	4.0	29	5.9	1.19	5	27
215550–113948	2153–115	GPS			1	1?	N	1?	0.37	4.85	25
221206+235540	2209+236	HFP	Q		5	12.6	6		1.18	5	6
221237+015251	4C+01.69	GPS	G		11	0.5	11	0.5	1.05	5	11
223834+124251	2236+124	GPS	Q		1, 29	5?	N	5?	0.33	5	27
225717+024317	2254+024	HFP	Q	2.081	5	19.5	6	60.1	0.274	5	6
232510–034446	2322–040	GPS	G		1, 29	1.4	4	1.4	0.91	2.7	4
232503+791716	2323+790	GPS	G		1, 29	?	N	?	1.136	1.4	19
233013+334838	2327+335	HFP	Q	1.809	5	5.6	6	15.7	0.558	5	6
233946–060412	4C–06.76	GPS	G		4	0.4	4	0.4	0.8	2.7	4
234029+264157	2337+264	GPS	Q		1, 29						
234403+822640	2342+821	GPS	Q	0.735	11, 1	0.5	11	0.9	1.28	5	11

Columns: (1) J2000 name. (2) B1950 or catalogue name. (3) GPS/HFP classification according to intrinsic peak frequency. (4) Optical identification: G = galaxy, Q = quasi-stellar object. (5) Redshift (p = photometric). (6) Reference where the source is listed as a GPS, and references for optical ID and redshift. (7 and 8) Observed frequency of the spectral peak and reference. Data from NED were used to estimate the spectral peak for those sources with no published measurements of the peak frequency. "?" means that confirmation of the radio spectral shape seems necessary. (9) Intrinsic frequency of the spectral peak. (10, 11 and 12) Flux density, frequency at which the flux density was measured, and reference.
References: 0 = This work. 1 = O'Dea et al. (1991), 2 = 2 Jy Sample: Morganti et al. (1993); Tadhunter et al. (1993); di Serego-Alighieri et al. (1994); Morganti et al. (1997), 3 = Edwards & Tingay (2004), 4 = Snellen et al. (2002), 5 = Tinti et al. (2005), 6 = Dallacasa et al. (2000), 7 = Augusto et al. (2006), 8 = Snellen et al. (1996), 9 = Becker et al. (1991), 10 = Kuehr et al. (1981), 11 = O'Dea (1998), 12 = Zensus et al. (2002), 13 = Marcha et al. (1996), 14 = Best et al. (2003), 15 = Xiang et al. (2006), 16 = CORALZ sample: Snellen et al. (2004), 17 = Torniainen et al. (2005), 18 = de Vries et al. (2000b), 19 = Condon et al. (1998), 20 = de Vries et al. (1995), 21 = Snellen et al. (1999), 22 = Beasley et al. (2002), 23 = Snellen et al. (2000), 24 = Xu et al. (1994), 25 = Griffith et al. (1994), 26 = Wright et al. (1994), 27 = Wright & Otrupcek (1990), 28 = De Breuck et al. (2002), 29 = de Vries et al. (1997), 30 = Snellen et al. (1998), 31 = Xiang et al. (2002), N = NASA/IPAC Extragalactic Database (NED).